# Anomalous Interlayer Transport of Quantum Hall Bilayers in the Strongly Josephson-Coupled Regime

Ding Zhang,* Werner Dietsche, and Klaus von Klitzing
*Max Planck Institute for Solid State Research, Heisenbergstrasse 1, D-70569 Stuttgart, Germany*
(Received 18 February 2016; published 2 May 2016)

We investigate Josephson coupling in a closely spaced quantum Hall bilayer. Reduction of the interlayer barrier from the widely used values of 10–12 nm to the present one of 8 nm leads to qualitatively different interlayer transport properties. The breakdown of interlayer coherence can be spatially confined in regions that are smaller than the device size. Such a spatial inhomogeneity depends crucially on the Josephson-coupling strength and can be removed by adding an in-plane magnetic field of about 0.5 T. At higher in-plane fields, the interlayer tunneling $I$-$V$ curve develops unexpected overshoot features. These results challenge current theoretical understanding and suggest that our bilayer system has entered a previously unexplored regime.

DOI: 10.1103/PhysRevLett.116.186801

Double layer electronic systems receive lasting attention, as their layer degree of freedom helps engender novel quantum phenomena [1–7] and inspires new experimental techniques [8–15]. One major focus of the research on bilayers is the realization of an excitonic Bose-Einstein condensate [2,16]. This condensate has been realized in a GaAs double quantum well system under a strong perpendicular magnetic field and is also predicted, but still remains elusive, in bilayer graphene [17–20]. In a GaAs bilayer system, when each layer is at a Landau level filling of $1/2$, electrons in one layer can pair up with vacant states, i.e., holes in the opposite layer, provided that the layer separation $d$ becomes comparable to the magnetic length $l_B$ ($d/l_B < 2$). This pairing gives rise to an exciton condensate. One key observation attesting to the formation of such a condensate was that of Josephson-like interlayer tunneling [3,21–23]. A dramatically enhanced interlayer conductance occurred at around zero bias. Once exceeding a critical current, the interlayer coherence breaks down and incoherent tunneling becomes dominant.

In earlier studies, the interlayer critical current reached only values on the order of tens of picoamperes. However, by slightly reducing the interlayer barrier (from $b = 12$ nm to $b = 10$ nm) or increasing the subband splitting energy $\Delta_{\mathrm{SAS}}$ (by a factor of 10), the critical current was greatly enhanced [24]. This enhancement has led to a number of intriguing observations [3,5]. It has also prompted further theoretical investigations [25–27]. Of special interest is the indication that, with an ever reducing interlayer barrier, the coherent tunneling may eventually transit to a different regime—the strong tunneling regime where novel phenomena are expected. Hyart and Rosenow [24] predicted that the transition occurs when the conductance of an independent domain becomes comparable to the conductance quantum $e^2/h$. On the other hand, Sodemann *et al.* [25] used a different approach and predicted that the threshold is related to a characteristic length $\lambda \propto 1/\Delta_{\mathrm{SAS}}$. The simple summation of nonlocal Josephson currents, which was experimentally observed [5,28], may be violated as $\lambda$ becomes smaller than the typical sample size. The thinnest bilayer samples ($b = 8$ nm) we addressed in previous works [29] may have already fallen into this category. The interlayer transport in the strong tunneling regime distinguishes itself by involving the breakdown process of the quantum Hall state.

Here, we report unusual interlayer transport properties observed in the quantum Hall bilayer with a barrier thickness of 8 nm. A specially designed contact geometry is employed to probe the interlayer voltages at different positions of the bilayer. The bilayer can be driven into spatial separation of coherent and incoherent regions. The sensitive dependence of this phenomenon on interlayer tunneling strength is verified by applying an in-plane magnetic field $B_{\parallel}$, which recovers the bilayer back to a uniform system at about 0.5 T. At higher in-plane fields ($B_{\parallel} \geq 3$ T), the Josephson current exhibits a gradual decrease and the interlayer $I$-$V$ acquires a sharp peak around zero bias. These behaviors deviate from present theoretical expectations and call for further investigations on the bilayer in the strongly coupled regime.

The bilayer studied here consists of two 19 nm wide GaAs quantum wells separated by an 8 nm thick AlAs/GaAs superlattice barrier. Each quantum well hosts electrons with a density of around $4 \times 10^{10}$ cm$^{-2}$ and a mobility of $5 \times 10^5$ cm$^2$/Vs. The electron density in each layer can be tuned with the help of a front and a back gate. The device is operated in the balanced regime with the same electron densities in each layer: between 2.2 and $3.2 \times 10^{10}$ cm$^{-2}$. Figure 1(a) schematically illustrates our specially designed Hall bar. The central region, controlled by the density tuning front and back gates, in which the $\nu_{\mathrm{tot}} = 1$ state would occur is contacted at six positions.

 

At each position, the contacting arm has a $Y$-shaped bifurcation [4,30]. Applying negative voltages to the small gates crossing either one of the branches, one selectively depletes the layers [31]. Each branch thus contacts a different layer. Tunneling current can then be injected to the $\nu_{\mathrm{tot}} = 1$ region of the top layer and can be withdrawn from the bottom layer at vertically overlapping positions (for example, $t1 \rightarrow b1$). If this pair of contacts is used for voltage sensing, the interlayer voltage can be measured without a possible contribution from the intralayer transport. The sample was mounted on a platform in a $^3$He/$^4$He dilution refrigerator (base temperature $\leq 20$ mK) that can be rotated *in situ* with an external motor. dc measurements were carried out in a four-terminal configuration at the center of the $\nu_{\mathrm{tot}} = 1$ quantum Hall plateau. An in-plane magnetic field component ($B_{\|}$) was introduced by rotating the sample while keeping the field component normal to the sample plane ($B_{\perp}$) fixed.

The thin-barrier bilayer exhibits an interlayer $I$-$V$ at $B_{\|} = 0$ T that reflects the quantum Hall breakdown. The involvement of such a breakdown process can be appreciated from the close similarity between the interlayer $I$-$V$ curve and the pure intralayer $I_{\mathrm{in}} - V_{\mathrm{in}}$ curve, which is captured in Fig. 1(b). Two interlayer $I$-$V$ characteristics are shown here. They are obtained by passing an interlayer current through one end of the Hall bar ($t6 \rightarrow b6$) and measuring voltages at two different pairs of contacts ($V_1$: $t1 - b1$ and $V_2$: $t2$-$b2$). The $I_{\mathrm{in}}$-$V_{\mathrm{in}}$ curve is obtained by flowing current solely in the bottom layer and measuring the voltage across the same layer ($I_{\mathrm{in}}$: $b6 \rightarrow b3$, $V_{\mathrm{in}}$: $b1$-$b2$). All three curves display a vertical increase of current around zero bias and the same bending where the voltage starts to increase rapidly. This bending signals the breakdown of the quantum Hall state as the intralayer voltage suddenly rises. However, the breakdown process in the bilayer is distinctly different from the single layer case. The same evolution seen in the $I_6$-$V_1$ and $I_6$-$V_2$ curves reflects this nontrivial nature. For a trivial resistor network, as shown in the inset to Fig. 1(b), the current would concentrate on one side (node 1) and only a small fraction of the current could reach node $N$. The net current in the region probed by the voltmeter $V_1$ (see Fig. 1(b) top) should be larger than the one close to the voltmeter $V_2$. With an increasing interlayer current, the region probed by the voltmeter $V_1$ should break down first. The $I_6$-$V_2$ curve would then show bending at a higher current.

The expected difference in the two interlayer $I$-$V$ curves seems to be confirmed once we reduce the effective layer spacing, $d/l_B$, slightly (from $d/l_B = 1.71$ to $d/l_B = 1.56$). Figure 1(c) shows that the tunneling characteristic of the $I_6$-$V_2$ curve now behaves strikingly different from the $I_6$-$V_1$ one. This contrast is, however, greater than what is expected from the simple resistor network. Instead of just displaying a higher breakdown current, the $I_6$-$V_2$ curve displays no obvious bending up to five times the breakdown current shown by the $I_6$-$V_1$ curve. By placing the source and drain on the opposite end ($I$: $t3 \rightarrow b3$), the two interlayer transport curves switch roles [Fig. 1(d)]; i.e., the $I_3$-$V_1$ curve becomes almost vertical instead. (The negative slope in the $I_3$-$V_1$ curve may arise from the area not controlled by the front and back gates [32].) The same dichotomy is obtained by choosing voltage sensing contacts on the opposite side of the Hall bar ($t5$-$b5$ and $t4$-$b4$), reversing the polarity of the $B$ field or exchanging the

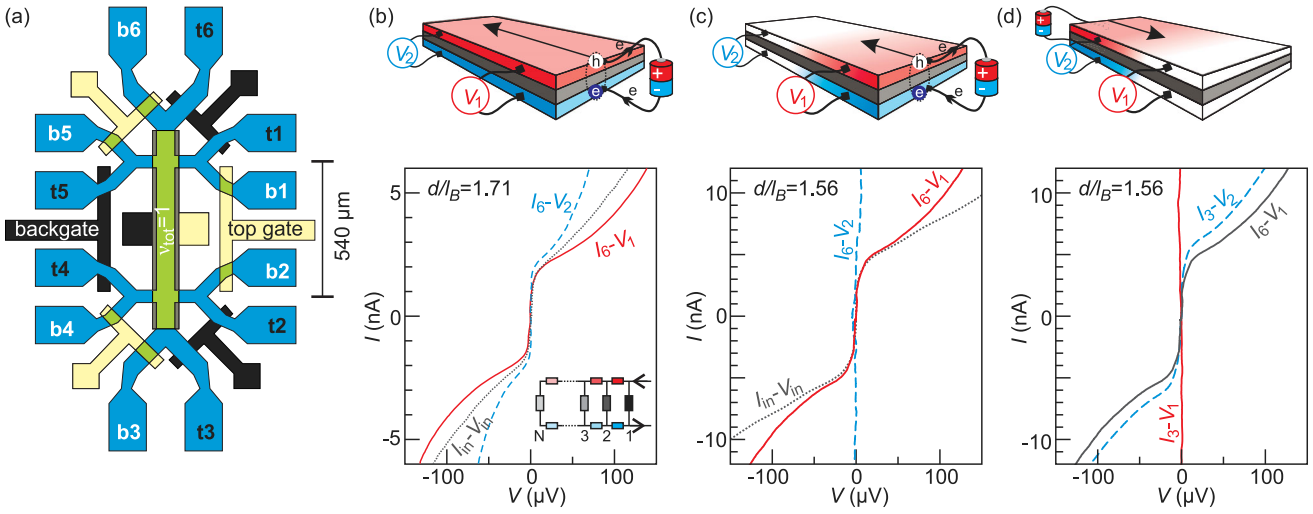


FIG. 1. (a) Sketch of the bilayer device. The $\nu_{\mathrm{tot}} = 1$ state forms in the central area. Contacts on the top (bottom) layer are marked as $t1$-$t6$ ($b1$-$b6$). (b)–(d) (Upper panels) Illustrated representations of the voltage distribution corresponding to different measurement configurations. (Lower panels) Tunneling $I$-$V$ characteristics and intralayer $I$-$V$ obtained at $d/l_B = 1.56$ and $d/l_B = 1.71$, respectively. The interlayer voltage $V_1$ ($V_2$) was measured between $t1$ ($t2$) and $b1$ ($b2$), while $I_6$ flows from $t6 \rightarrow b6$ in (b),(c) and $I_3$: $t3 \rightarrow b3$ in (d). The intralayer voltage $V_{\mathrm{in}}$ was measured between $b1$ and $b2$ with $I_{\mathrm{in}}$: $b6 \rightarrow b3$. The inset in (b) shows a resistor network with the vertical (horizontal) resistors representing the interlayer (intralayer) resistance components.

source and the drain with a pair of voltage probes ($t6$, $b6 \leftrightarrow t1$, $b1$). An illustrated representation of this spatial dependence is shown in the upper panels of Figs. 1(c) and 1(d). The color shaded sections represent regions where large interlayer voltages can build up after reaching the critical current. The white region remains coherent as there is no interlayer voltage. In addition, a careful comparison between the $I_6$-$V_1$ and $I_3$-$V_2$ curves in Fig. 1(d) reveals that the magnitude of the critical current varies, reflecting the local nature of the breakdown process.

The collective nature of the quantum Hall bilayer is essential for understanding the nonlocal [Fig. 1(b)] to local [Fig. 1(c)] transition of the breakdown process. In our experimental configuration, injecting an electron into one layer is accompanied by withdrawing another one from the opposite layer at vertically the same position. The latter process is equivalent to the injection of a hole. Together with the electron in the first layer, excitons, which are neutral, propagate into the bilayer without dissipation [shown in Figs. 1(b) and 1(c)]. Only when the exciton current becomes too large does the dissipative process set in and the exciton condensate break down [6,29]. By adopting this exciton injection picture, we interpret the strong position dependence shown in Figs. 1(c) and 1(d) as evidence of the formation of exciton domains. Because of the strongly enhanced interlayer coupling, excitons may get confined in domains that are smaller than the sample. The $I_6$-$V_1$ curve in Fig. 1(c) therefore represents transport in one such domain. Breakdown of the interlayer coherence is confined in this domain and the region probed by $V_2$ is unaffected. The transition of the situation from Fig. 1(c) to Fig. 1(b) can then be understood as an evolution from a scenario of multidomains to the situation of a single domain when the effective interlayer spacing ($d/l_B$) increases.

In order to continuously tune the interlayer tunneling strength, we introduce an in-plane $B$ field ($B_\parallel$). Previous experiments [33] have demonstrated the suppression of the Josephson current by one order of magnitude when applying $B_\parallel = 0.5$ T. Calculations [24] have explained this by assuming a coherence network with a typical impurity related length scale of much less than 1 $\mu$m [34,35] in which the Josephson current is suppressed. The domains seen in the data of Fig. 1 are much larger than this and must therefore have a different origin. We adopt the characteristic length $\lambda$ proposed by Sodemann *et al.* [25]. They suggest that a domain has a typical length of 0.1 to 1 mm, comparable to the sample size. This length scale increases when reducing the interlayer coupling. For our bilayer with spatially nonuniform transport, a transition to a uniform regime is anticipated by enlarging the domain size. This could be achieved by applying $B_\parallel$. Figure 2 displays just such a transition. The $I$-$V$ curves are measured using the same configuration as for the data in Fig. 1(c). At $B_\parallel = 0.21$ T, the $I_6$-$V_2$ curve starts to exhibit shoulders at certain currents (marked as $\pm I_{2,c}$). Still, the shoulders indicate a much larger critical current than the $I_6$-$V_1$ curve does. The difference gets smaller by going to $B_\parallel = 0.37$ T [Fig. 2(b)] and vanishes at $B_\parallel$ above 0.6 T [Figs. 2(c) and 2(d)]. Again, this tuning is remarkable and speaks against a trivial explanation. In a simple resistor network, tuning the ratio between the inter- and intralayer resistances [inset to Fig. 1(b)] would never remove the difference between currents at $V_1$ and $V_2$. It is worth pointing out that, unlike the situation in Fig. 1(b), the two overlapping interlayer $I$-$V$ curves in Fig. 2(c) are fully enveloped by the intralayer data. The Josephson current is now decoupled from the quantum Hall breakdown.

Because of the involvement of quantum Hall breakdown, the Josephson-coupling strength cannot be directly calculated from the critical current at $B_\parallel = 0$ T. We employ the formula developed by Hyart and Rosenow (H-R) to estimate this coupling strength [36]. For bilayers with thicker barriers, the theoretically prescribed $I_c$-$B_\parallel$ curve can quantitatively reproduce the experimental results. The empty triangles in Fig. 3(a) are experimentally determined critical currents from another bilayer with a barrier thickness of $b = 10$ nm. The dotted curve is a calculation which reproduces the fast decay process. The bilayer used here ($b = 8$ nm) is in the strong tunneling regime that may not be fully captured by the H-R theory. However, interlayer

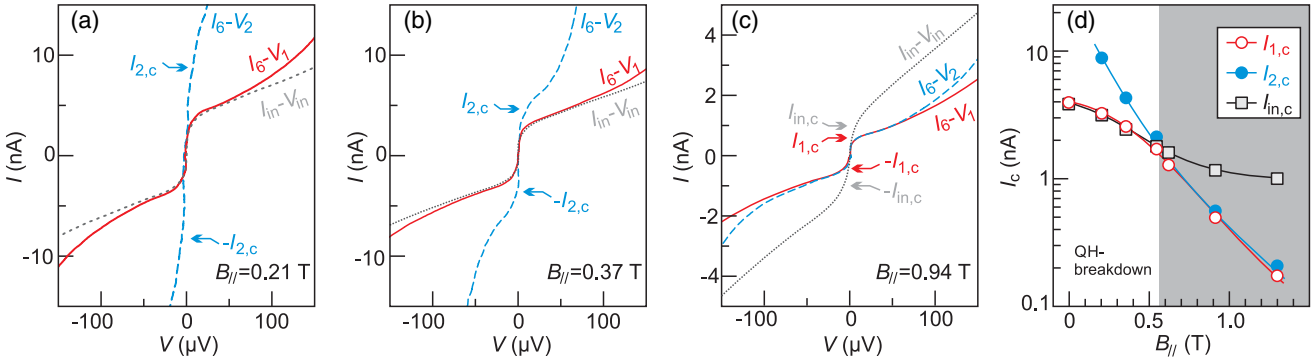


FIG. 2. (a)–(c) Tunneling $I$-$V$ characteristics and intralayer $I$-$V$ obtained at different $B_\parallel$'s. The $d/l_B$ ratio is 1.56. (d) Critical currents as a function of $B_\parallel$ summarized for $d/l_B = 1.56$.

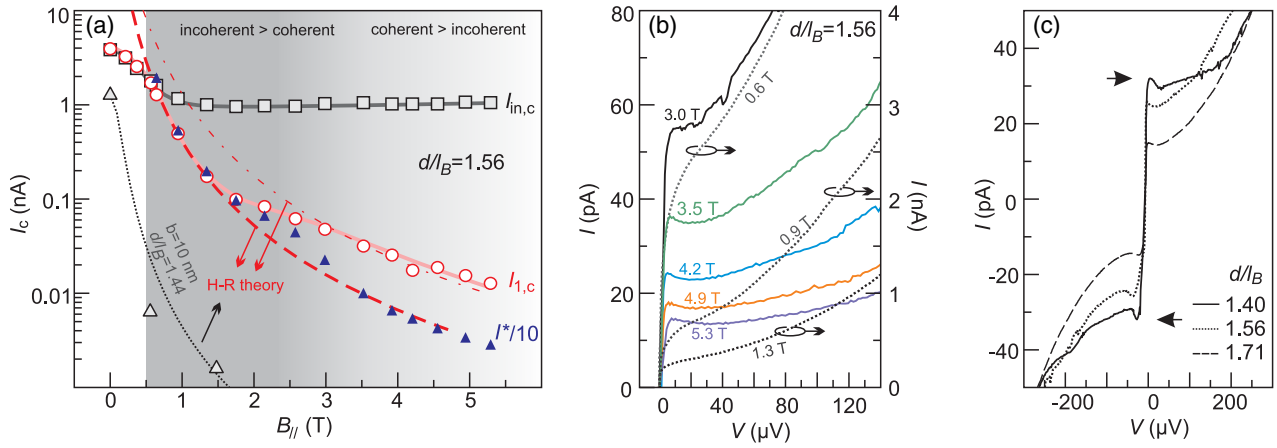


FIG. 3. (a) Critical currents as a function of $B_\parallel$. Here $I_{1,c}$ is the Josephson critical current, $I_{\mathrm{in},c}$ is the intralayer critical current. Filled triangles indicate an incoherent tunneling current at 200 $\mu$V. Empty triangles show the Josephson critical current from another bilayer with a thicker barrier ($b = 10$ nm). Solid lines are a guide for the eye. The dashed and dotted lines represent the theoretically expected Josephson current as a function of $B_\parallel$. Parameters (see Ref. [36]) used are (dashed and dash-dotted lines) $I_0 = 33$ nA, $V_0 = 100$ $\mu$V, $\alpha = 0.01$, $d = 27$ nm, $\xi = 150$ nm for the dashed and $\xi = 100$ nm for the dash-dotted line, and (dotted line) $I_0 = 0.44$ nA, $V_0 = 100$ $\mu$V, $\alpha = 0.01$, $d = 29$ nm, $\xi = 150$ nm. (b) Interlayer Josephson tunneling at $d/l_B = 1.56$ for various $B_\parallel$ values. (c) Interlayer Josephson tunneling at large in-plane $B$ fields obtained for three $d/l_B$ ratios ($B_\parallel = 4.3$ T for $d/l_B = 1.40$ and $d/l_B = 1.71$; $B_\parallel = 4.2$ T for $d/l_B = 1.56$).

coupling at a large $B_\parallel$ should be suppressed to the level that the perturbative treatment of H-R theory is still valid. The calculated $I_c$-$B_\parallel$ relation is shown as the dashed and dash-dotted curves. We have adjusted the parameters (mainly $I_0$ and the coherent length $\xi$ in Ref. [36]) such that the curves fit to our data in the regime not governed by the quantum Hall breakdown. Two calculated $I_c$-$B_\parallel$ curves with different coherence lengths ($\xi = 150$ nm for the dashed curve and 100 nm for the dash-dotted curve) are shown in Fig. 3(a). They overlap partially with the data points in the range either from 0.6 to about 2 T or above 3 T. The experimental data have a more complicated evolution as a function of $B_\parallel$. Nevertheless, the theoretical fittings all point to an interlayer conductance at zero bias of around 1700 $e^2/h$ for $B_\parallel = 0$ T. A 6 $\mu$m-sized domain, which is much smaller than our sample, already has conductance of $e^2/h$. It confirms that our bilayer is in the strong tunneling regime where the theory is not fully developed [24].

In addition to the quantitative difference between experiment and theory shown in Fig. 3(a), we observed a qualitative change of the $I$-$V$ curves. Figure 3(b) shows that the $I$-$V$ curves have rounded steps around zero bias at intermediate in-plane $B$ fields but exhibit a small peak at around 10 $\mu$V once exceeding $B_\parallel \sim 3$ T. This sharp feature becomes more apparent as the system is tuned deeper into the coherent phase [indicated by arrows in Fig. 3(c)]. The emergence of the peaks is accompanied by a rapid drop of the slope at large bias, indicating a severely suppressed incoherent tunneling. For a quantitative comparison, we ascribe the interlayer current measured at 200 $\mu$V to the incoherent tunneling. The coherent Josephson process contributes little at this large bias. Filled triangles in Fig. 3(a) represent the incoherent tunneling current ($I^*$) as a function of $B_\parallel$. Clearly, $I^*$ drops faster with an increasing $B_\parallel$ than $I_c$ does for $B_\parallel > 2$ T. We therefore mark the $B$-field ranges in Fig. 3(a) as strong and weak incoherent regimes, respectively. The small peaks in the $I$-$V$ curves may already be present at intermediate fields but are masked by the incoherent tunneling. The persistence of the small peaks up to strong in-plane fields remains puzzling. Previous experiments on bilayers with thicker barriers reported that the sharp features vanish once $B_\parallel$ exceeds about 0.5 T [37]. Transport properties in a strongly coupled bilayer seem to be qualitatively different from the ones in bilayers with thicker barriers.

To summarize, a quantum Hall bilayer with a drastically reduced interlayer distance hosts signatures of domain formation predicted by theory. The domain size crucially depends on the interlayer coupling strength. Uniform interlayer transport is retained by either increasing the effective interlayer spacing (the $d/l_B$ ratio) or applying a small in-plane magnetic field ($\geq 0.5$ T). We obtain the evolution of interlayer transport over an extended range of in-plane magnetic fields (0–5.3 T). Data at high $B_\parallel$'s call for further theoretical development of the quantum Hall bilayer in the strong tunneling regime.

This project was supported by the BMBF (German Ministry of Education and Research) Grants No. 01BM456 and No. 01BM900. We thank Jurgen Smet, Bernd Rosenow, Lars Tiemann, Inti Sodemann, and Allan MacDonald for the helpful discussions. We would like to

acknowledge Joseph Falson for his critical reading of the manuscript. The sample design is based on earlier works of Lars Tiemann. Maik Hauser and Marion Hagel kindly provided technical assistance.

*Present address: State Key Laboratory of Low-Dimensional Quantum Physics, Department of Physics, Tsinghua University, Beijing 100084, China.

[1] J. P. Eisenstein, G. S. Boebinger, L. N. Pfeiffer, K. W. West, and S. He, Phys. Rev. Lett. **68**, 1383 (1992).
[2] J. P. Eisenstein and A. H. MacDonald, Nature (London) **432**, 691 (2004).
[3] L. Tiemann, W. Dietsche, M. Hauser, and K. von Klitzing, New J. Phys. **10**, 045018 (2008).
[4] Y. Yoon, L. Tiemann, S. Schmult, W. Dietsche, K. von Klitzing, and W. Wegscheider, Phys. Rev. Lett. **104**, 116802 (2010).
[5] X. Huang, W. Dietsche, M. Hauser, and K. von Klitzing, Phys. Rev. Lett. **109**, 156802 (2012).
[6] D. Nandi, A. D. K. Finck, J. P. Eisenstein, L. N. Pfeiffer, and K. W. West, Nature (London) **488**, 481 (2012).
[7] L. Tiemann, W. Wegscheider, and M. Hauser, Phys. Rev. Lett. **114**, 176804 (2015).
[8] J. P. Eisenstein, L. N. Pfeiffer, and K. W. West, Phys. Rev. Lett. **68**, 674 (1992).
[9] A. Sciambi, M. Pelliccione, M. P. Lilly, S. R. Bank, A. C. Gossard, L. N. Pfeiffer, K. W. West, and D. Goldhaber-Gordon, Phys. Rev. B **84**, 085301 (2011).
[10] S. Kim, I. Jo, D. C. Dillen, D. A. Ferrer, B. Fallahazad, Z. Yao, S. K. Banerjee, and E. Tutuc, Phys. Rev. Lett. **108**, 116404 (2012).
[11] R. V. Gorbachev, A. K. Geim, M. I. Katsnelson, K. S. Novoselov, T. Tudorovskiy, I. V. Grigorieva, A. H. MacDonald, S. V. Morozov, K. Watanabe, T. Taniguchi and L. A. Ponomarenko, Nat. Phys. **8**, 896 (2012).
[12] L. Britnell, R. V. Gorbachev, A. K. Geim, L. A. Ponomarenko, A. Mishchenko, M. T. Greenaway, T. M. Fromhold, K. S. Novoselov, and L. Eaves, Nat. Commun. **4**, 1794 (2013).
[13] T. Roy, L. Liu, S. de la Barrera, B. Chakrabarti, Z. R. Hesabi, C. A. Joiner, R. M. Feenstra, G. Gu, and E. M. Vogel, Appl. Phys. Lett. **104**, 123506 (2014).
[14] D. Zhang, X. Huang, W. Dietsche, K. von Klitzing, and J. H. Smet, Phys. Rev. Lett. **113**, 076804 (2014).
[15] K. Lee, B. Fallahazad, J. Xue, D. C. Dillen, K. Kim, T. Taniguchi, K. Watanabe, and E. Tutuc, Science **345**, 58 (2014).
[16] J. Eisenstein, Annu. Rev. Condens. Matter Phys. **5**, 159 (2014).
[17] J. Su and A. H. MacDonald, Nat. Phys. **4**, 799 (2008).
[18] C.-H. Zhang and Y. N. Joglekar, Phys. Rev. B **77**, 233405 (2008).
[19] A. Pikalov and D. V. Fil, Nanoscale Res. Lett. **7**, 145 (2012).
[20] A. Perali, D. Neilson, and A. R. Hamilton, Phys. Rev. Lett. **110**, 146803 (2013).
[21] X. G. Wen and A. Zee, Phys. Rev. B **47**, 2265 (1993).
[22] Z. F. Ezawa and A. Iwazaki, Phys. Rev. B **47**, 7295 (1993).
[23] I. B. Spielman, J. P. Eisenstein, L. N. Pfeiffer, and K. W. West, Phys. Rev. Lett. **84**, 5808 (2000).
[24] T. Hyart and B. Rosenow, Phys. Rev. B **83**, 155315 (2011).
[25] I. Sodemann, H. Chen, and A. H. MacDonald, arXiv: 1411.0008.
[26] O. Kyriienko, K. Wierschem, P. Sengupta, and I. A. Shelykh, Europhys. Lett. **109**, 57003 (2015).
[27] Q.-D. Jiang, Z.-q. Bao, Q.-F. Sun, and X. C. Xie, Sci. Rep. **5**, 11925 (2015).
[28] D. Nandi, T. Khaire, A. D. K. Finck, J. P. Eisenstein, L. N. Pfeiffer, and K. W. West, Phys. Rev. B **88**, 165308 (2013).
[29] D. Zhang, X. Huang, W. Dietsche, M. Hauser, and K. von Klitzing, Phys. Rev. B **90**, 085436 (2014).
[30] M. Kellogg, J. P. Eisenstein, L. N. Pfeiffer, and K. W. West, Phys. Rev. Lett. **93**, 036801 (2004).
[31] H. Rubel, A. Fischer, W. Dietsche, K. von Klitzing, and K. Eberl, Mater. Sci. Eng. B **51**, 207 (1998).
[32] L. Tiemann, Ph.D. thesis, Max Planck Institute for Solid State Research, 2008.
[33] I. B. Spielman, J. P. Eisenstein, L. N. Pfeiffer, and K. W. West, Phys. Rev. Lett. **87**, 036803 (2001).
[34] H. A. Fertig and G. Murthy, Phys. Rev. Lett. **95**, 156802 (2005).
[35] P. R. Eastham, N. R. Cooper, and D. K. K. Lee, Phys. Rev. B **80**, 045302 (2009).
[36] We used the formula [24]

$$I(V,B_\parallel) = I_0 \int\int dq dR \left(\frac{\alpha}{\alpha^2+(V/V_0-q)^2} - \frac{\alpha}{\alpha^2+(V/V_0+q)^2}\right) \times R\exp(-R) J_0(qR) J_0\left(2\pi \frac{eB_\parallel \xi d}{h} R\right). \quad (1)$$

Here, $\alpha$ is a fitting parameter, $\xi$ is the coherent length, and $d$ is the interlayer distance. The $B_\parallel$ dependence of the critical Josephson current is essentially governed by the last term in the equation. The term $eB_\parallel \xi d/h$ plays the same role of suppressing the critical current as in a superconductor Josephson junction. The difference here is that the bilayer consists of multiple parallel junctions with a length scale of $\xi$. Each junction encloses in-plane flux quanta on the order of $\Phi = B_\parallel \xi d$. Similar to a superconductor junction, the tunneling current in the quantum Hall bilayer decreases with an increasing ratio of $\Phi/\Phi_0$ (here, $\Phi_0 = h/e$). The Fraunhofer diffraction pattern is averaged out due to the presence of many junctions with random phases. $I$-$V$ curves can be obtained by numerically solving the integration at fixed numbers of $B_\parallel$. We then extract the maximum currents around zero bias as the critical currents ($I_c$).
[37] I. B. Spielman, Ph.D. thesis, California Institute of Technology, 2004. The tunneling data at finite in-plane magnetic fields is reproduced in Ref. [24].